NeuroImage 53 (2010) 1197–1207

Contents lists available at ScienceDirect

NeuroImage

journal homepage: www.elsevier.com/locate/ynimg

Network-based statistic: Identifying differences in brain networks

Andrew Zalesky [a,b,*], Alex Fornito [a,c], Edward T. Bullmore [c]

[a] Melbourne Neuropsychiatry Centre, Department of Psychiatry, The University of Melbourne and Melbourne Health, Australia
[b] Department of Electrical and Electronic Engineering, Melbourne School of Engineering, The University of Melbourne, Australia
[c] Behavioural and Clinical Neuroscience Institute, University of Cambridge, Department of Psychiatry, Herchel Smith Building for Brain and Minds Sciences, Cambridge Biomedical Campus, Cambridge, UK

ARTICLE INFO

Article history:
Received 25 April 2010
Revised 31 May 2010
Accepted 16 June 2010
Available online 25 June 2010

Keywords:
Network
Graph
Functional connectivity
Structural connectivity
Resting-state fMRI
Diffusion MRI
Clustering
Schizophrenia

ABSTRACT

Large-scale functional or structural brain connectivity can be modeled as a network, or *graph*. This paper presents a statistical approach to identify connections in such a graph that may be associated with a diagnostic status in case-control studies, changing psychological contexts in task-based studies, or correlations with various cognitive and behavioral measures. The new approach, called the network-based statistic (NBS), is a method to control the family-wise error rate (in the weak sense) when mass-univariate testing is performed at every connection comprising the graph. To potentially offer a substantial gain in power, the NBS exploits the extent to which the connections comprising the contrast or effect of interest are interconnected. The NBS is based on the principles underpinning traditional cluster-based thresholding of statistical parametric maps. The purpose of this paper is to: (i) introduce the NBS for the first time; (ii) evaluate its power with the use of receiver operating characteristic (ROC) curves; and, (iii) demonstrate its utility with application to a real case-control study involving a group of people with schizophrenia for which resting-state functional MRI data were acquired. The NBS identified a expansive dysconnected subnetwork in the group with schizophrenia, primarily comprising fronto-temporal and occipito-temporal dysconnections, whereas a mass-univariate analysis controlled with the false discovery rate failed to identify a subnetwork.

Introduction

It has become fashionable in the field of neuroimaging to model and analyze the brain in terms of a network. With the popularization of complex systems theory and the emergence of network science, *graph* models have become especially popular for they open up the door to a systems-theoretic description of the brain. That is, a description where brain complexity can be reduced to an account of the interactions between basic neuronal elements.

The graph model of the brain is an abstract structure used to represent pairwise relations between interregional ensembles of neuronal elements, referred to as *nodes*. These pairwise relations, or *links*, can either be of a functional origin and represent coherent physiological activity between neural ensembles, or they can be of a structural origin and represent anatomical connections formed by white-matter axonal fiber tracts.

The graph model has been used in neuroimaging research as a framework to test the structure-function hypothesis (Honey et al., 2009, 2010; Ramani et al., 2004; Skudlarski et al., 2008; Sporns et al., 2000) and as a methodological tool to examine brain network organization, topology and complex dynamics (Bullmore et al., 2009; Hagmann et al., 2008; Sporns et al., 2004). It has been found that the human brain exhibits various nontrivial organizational and topological properties, such as: assortativity, centrality, clustering, efficiency, hierarchy, hubs, modularity, robustness, small-worldness, synchronizability, etc. (see Bullmore & Sporns, 2009, for a review). Differences in one or more of these properties have been found in people with Alzheimer's disease (He et al., 2008; Stam et al., 2007), attention-deficit disorder (Wang et al., 2009), multiple sclerosis (He et al., 2009) and schizophrenia (Bassett et al., 2008, 2009; Liu et al., 2008; Rubinov et al., 2009) as well as associations with age and gender (Gong et al., 2009; Wang et al., 2010), and intelligence (van den Heuvel et al., 2009; Li et al., 2009).

The graph model also provides an ideal framework to identify functional or structural connections associated with a particular effect or contrast of interest; for example, a group difference in a case-control comparison, a difference due to changing task conditions in a functional paradigm, or a correlation with some clinical measure. To this end, mass-univariate testing of the hypothesis is undertaken, after which the family-wise error rate (FWE) is controlled with a generic procedure, such as the false discovery rate (FDR) (Genovese et al., 2002). Specifically, a test

* Corresponding author. Melbourne Neuropsychiatry Centre, Department of Psychiatry, The University of Melbourne and Melbourne Health, Australia.
E-mail address: azalesky@unimelb.edu.au (A. Zalesky).

1053-8119/$ – see front matter © 2010 Elsevier Inc. All rights reserved.
doi:10.1016/j.neuroimage.2010.06.041

statistic and corresponding p-value is independently computed for each link based on the strength of the pairwise association the link represents. The strength of a pairwise association between nodes is usually measured as the value of temporal correlation (functional) or the total number of interconnecting streamlines (structural).

The advantage of this approach is that it does not require interpretation of any abstract organizational or topological properties. Its main disadvantage though is the inherent massive number of multiple comparisons that must be performed. To appreciate the massiveness of the multiple comparisons problem, consider the following: performing a mass-univariate analysis on a statistical parametric map involves in the order of thousands of multiple comparisons, say 1000 voxels for concreteness; however, if each of these 1000 voxels delineates a unique node, the number of multiple comparisons increases to a staggering $\binom{1000}{2} = 499,500$ connections. With such a large number of multiple comparisons, together with a potentially low contrast-to-noise ratio, mass-univariate testing may not offer sufficient power.

Note that when the hypothesis of interest is associated with a *global* network measure, the issue of multiple comparisons does not arise. This paper exclusively focuses on multiple hypothesis testing, where one instead tests the hypothesis of interest at each network connection, thereby introducing more localizing power at the cost of a massive number of multiple comparisons.

The main contribution of this paper is to present a potentially more powerful method to control the FWE when performing this kind of analysis. The new method is called the network-based statistic (NBS) and can be thought of as a translation of conventional cluster statistics (Bullmore et al., 1999; Nichols & Holmes, 2001) to a graph. In brief, the NBS operates as follows: foremost, the test statistic computed for each link is thresholded to construct a set of suprathreshold links. Any connected structures, or *components* in graph parlance, that may be present in the set of suprathreshold links are then identified. A p-value is assigned to each identified component by indexing its size with the null distribution of maximal component size.

In this way, the NBS attempts to utilize the presence of any structure exhibited by the connections comprising the effect or contrast of interest to yield greater power than what is possible by independently correcting the p-values computed for each link using a generic procedure to control the FWE. In this paper, any procedure for controlling the FWE that treats each link independently will be referred to as a *link-based controlling procedure*, or simply *link-based FWE control*.

The NBS is *not* intended as a replacement for link-based FWE control. In particular, the NBS offers no power if the links associated with the contrast or effect of interest are in isolation of each other and do not form any connected structures. Therefore, in addition to introducing and demonstrating the utility of the NBS, one of the main purposes of this paper is to undertake a quantitative evaluation of the gain (and potential loss) in statistical power offered by our new approach. To this end, the paper comprises three parts: Section 2: introduction of the NBS by way of an illustrative example; Section 3: evaluation of the power of the NBS with use of receiver operating characteristic (ROC) curves; and, Section 4: demonstration of the NBS in the context of a real case-control study involving resting-state functional MRI data acquired in 12 people with schizophrenia and 15 controls.

Methods

To use the NBS, one must first generate a connectivity matrix for each subject. The connectivity matrix is intrinsic to the graph model and its computation has been described in (Bullmore & Sporns, 2009) and many references therein. As such, the main focus of this section is the implementation of the NBS *after* the connectivity matrix stage has been reached, though a brief overview of getting to this stage is provided for completeness.

Connectivity matrix

To define the graph model, it is first necessary to delineate an appropriate set of nodes. The choice of nodes is dependent on the imaging modality. For electroencephalography or magnetoencephalography, a natural choice is the set of array electrodes or scalp sensors, while in the case of functional, structural and diffusion MRI, a node usually represents a contiguous group of voxels, or possibly a single voxel. In this case, delineating a set of nodes involves subdividing the whole cortex into a set of regions either randomly, with reference to a predefined histological or functional subdivision, or simply by defining every cortical voxel to constitute a unique node (van den Heuvel et al., 2008). For example, the automated anatomical labeling (AAL) atlas (Tzourio-Mazoyer et al., 2002), a gross functional subdivision of the cortex, was used to delineate the set of nodes for the resting-state study presented in this paper (see Section 4). Further discussion on the choice of nodes is provided in Zalesky et al., (2010).

The next step is to estimate a continuous measure of pairwise association between nodes. This measure is stored in a symmetric $N \times N$ connectivity matrix, where N is the total number of nodes. Each row/column of the connectivity matrix corresponds to a distinct node, such that position (i,j) uniquely stores the measure of association between the ith and jth nodes.

The appropriate measure of association largely depends on the imaging modality. In the case of functional MRI, electroencephalography or magnetoencephalography, temporal correlations (Achard et al., 2006; Deuker et al., 2009; Fair et al., 2009; Hayasaka & Laurienti, 2010; Honey et al., 2009; Li et al., 2009) or mutual information (Bassett et al., 2009) in the node-averaged signals are computed. Any temporal correlation provides evidence for coherent neural dynamics and thereby determines the extent to which nodes are functionally connected. Therefore, in this case, the connectivity matrix is invariably populated with some kind of measure of correlation.

In the case of diffusion MRI, associations are of a structural origin and represent anatomical connections formed by white-matter axonal fiber tracts. With the use of a tractography (Basser et al., 2000; Conturo et al., 1999), hundreds of thousands of streamlines are generated to etch out the trajectories of these fiber tracts and the association between a pair of nodes is measured by the number of streamlines via which they are interconnected (Gong et al., 2009; Hagmann et al., 2007, 2008; Itturia-Medina et al., 2008; Li et al., 2009; Skudlarski et al., 2008; Zalesky et al., 2010), or in some cases, a pseudo-measure of the tract-averaged anisotropy (Robinson et al., 2010) or an estimate of fiber bundle cross-sectional area (Zalesky & Fornito, 2009). Alternatively, cross-subject correlation in estimates of cortical thickness or volume, derived from structural MRI, provide an alternative means to measure structural associations between nodes (Bassett et al., 2008; He et al., 2007, 2008, 2009).

The next step in a typical analysis would be to apply a threshold to each element of the connectivity matrix and thereby define a sparse graph; that is, a graph in which links are only drawn between those pairs of nodes demonstrating a measure of association exceeding the predefined threshold. Unfortunately, this step introduces a potential confound if the properties of several graphs are to be compared in the context of a case-control study. In particular, applying the same threshold to several connectivity matrices is likely to produce different levels of sparsity (i.e. different number of links), and thus it is not possible to rule out systematic sparsity differences as the root cause of any group differences in topological or organizational properties. While graphs can be matched in terms of sparsity, this necessitates selection of a distinct threshold for each connectivity matrix, which in itself raises potential concerns. An advantage of the NBS is that it operates directly on the raw measure of connectivity, rather than a binary adjacency matrix.

Network-based statistic

For ease of exposition, the NBS is described here within the framework of a generic case-control study. However, it is important to note that the NBS is easily generalizable to multifactorial designs stemming from, for example, task-based functional MRI studies, as we have recently demonstrated in Fornito et al., 2010.

The purpose of the NBS in the context of a case-control study is to identify any pairwise associations that are significantly different between groups. In the graph model, a pairwise association manifests as a "connection," or *link*, between a distinct pair of nodes. An $N \times N$ connectivity matrix stores the estimates of a total of $N(N-1)/2$ unique pairwise associations. For each of these associations, the test statistic of interest is calculated independently using the values stored in each subject's connectivity matrix. In some circumstances, it may be appropriate to first transform the raw measure of association; for example, Fisher's *r*-to-*z* transform can be applied to a correlation based measure of association to ensure normality. This is not a specific requirement of the NBS, which is a nonparametric technique, but yields a sensible measure of variation to which a threshold can be applied.

The NBS seeks to identify any potential connected structures formed by an appropriately chosen set of suprathreshold links. The topological extent of any such structure is then used to determine its significance. This process is performed as follows: the test statistic computed for each pairwise association is thresholded to construct a set of suprathreshold links. Any connected components that may be present in the set of suprathreshold links are then identified using a breadth first search (Ahuja et al., 1993) and the number of links they comprise, or their *size*, is stored.

Permutation testing is used to ascribe a *p*-value controlled for the FWE to each connected component based on its size. A total of M random permutations are generated independently, where for each permutation, the group to which each subject belongs is randomly exchanged. For each permutation, the test statistic of interest is recalculated, after which the same threshold is applied to define a set of suprathreshold links. The maximal component size in the set of suprathreshold links derived from each of the M permutations is then determined and stored, thereby yielding an empirical estimate of the null distribution of maximal component size. Finally, the *p*-value of an observed component of size k is estimated by finding the total number of permutations for which the maximal component size is greater than k and normalizing by M. This kind of permutation testing is not new and is synonymous with conventional cluster-based thresholding of statistical parametric maps (Bullmore et al., 1999; Hayasaka & Nichols, 2004; Nichols & Holmes, 2001). The novelty here is in the translation and application of this approach to the graph model (see Fig. 1). The approach can also be straightforwardly generalized to multifactorial designs (Suckling & Bullmore, 2004).

To implement the NBS, an algorithm is required to compute the set of all connected components in a graph. This can be achieved in a runtime of $\mathcal{O}(N+L)$ using a breadth-first search (Hopcroft & Tarjan, 1973), where N is the number of nodes and L is the number of suprathreshold links. This is repeated for M permutations to estimate the null distribution, thereby yielding a total runtime of $\mathcal{O}(M(N+L))$. In practice, the majority of runtime is devoted to computing the test statistic of interest at each link.

Relation to link-based FWE control

Instead of the NBS, an alternative is to apply a generic procedure, most likely the FDR, to control for the massive number of multiple comparisons. In this context, the FDR is referred to as a link-based controlling procedure because each link is treated independently for the sake of FWE control. Note that the FDR controls the FWE in the weak sense (Nichols & Hayasaka, 2003). The NBS is not intended as a replacement for link-based controlling procedures such as the FDR, it is rather a complementary procedure that can offer substantially greater power if the connections associated with the contrast or effect of interest are interconnected to form a structure; or more precisely, a connected component. The underlying principle behind the NBS is to utilize the presence of any such components to potentially yield greater power than what is possible by independently correcting the *p*-values computed for each link. The NBS offers the greatest gain in power when the link-based *p*-values associated with the contrast are marginal, usually due to a low contrast-to-noise ratio, but are interconnected to form components. As the extent (size) of such a component decreases, it becomes more difficult to identify with the NBS, until the NBS is utterly powerless in the extreme case when the component comprises a single isolated link. As the contrast-to-noise ratio increases, the NBS continues to perform well, but link-based FWE control is then likely to perform just as well. These qualitative remarks are quantified in Section 3.

Finally, it is important to remark that the NBS is not entirely equivalent to link-based FWE control. With a link-based controlling procedure, the null hypothesis can be rejected on a link-by-link basis. With the NBS on the other hand, the null hypothesis can only be rejected on a component-by-component basis. Hence, with the NBS, it is never possible to declare individual links as being significant, only the component to which they belong can be declared significant. In this way, the NBS offers weak control over the FWE. Any significant result therefore provides evidence against the omnibus null hypotheses; however, because the false positive rate is not controlled at the link level, as would be required by *strong* control of FWE (Nichols & Hayasaka, 2003), individual links cannot be declared significant. This means the potential gain in power offered by the NBS comes at a price: localizing resolution is coarsened from the scale of a link to the scale of a component.

Illustrative example

To conclude this section, an illustrative example is presented in Fig. 2 to demonstrate the gain in power offered by the NBS relative to link-based FWE control, in a situation that is suited to the NBS; namely, a relatively low contrast-to-noise ratio of unity and a contrast that is defined by a set of links that form a single connected component.

For the purpose of the example, a between group difference was simulated in which a connected component, referred to as the *contrast*, was "disrupted" in one of the two groups. In one group, the measure of association assigned to each link was sampled from a Gaussian distribution of zero mean and unity variance. In the other group, sampling was also from a Gaussian distribution of unity variance, but with unity mean if the link comprised the contrast, otherwise with a

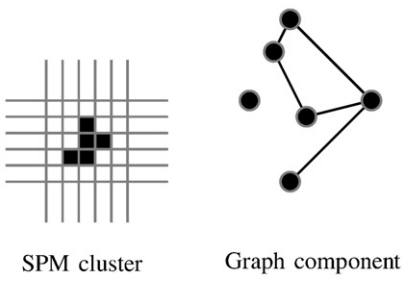

Fig. 1. The equivalence between a cluster in a statistical parametric map (left) and a component in a graph (right). Both are of extent five: the cluster comprises five voxels, while the component comprises five links. Note that a cluster is defined by spatial contiguity of suprathreshold voxels in physical image space, whereas a graph component is defined by interconnectedness of suprathreshold links in topological space.

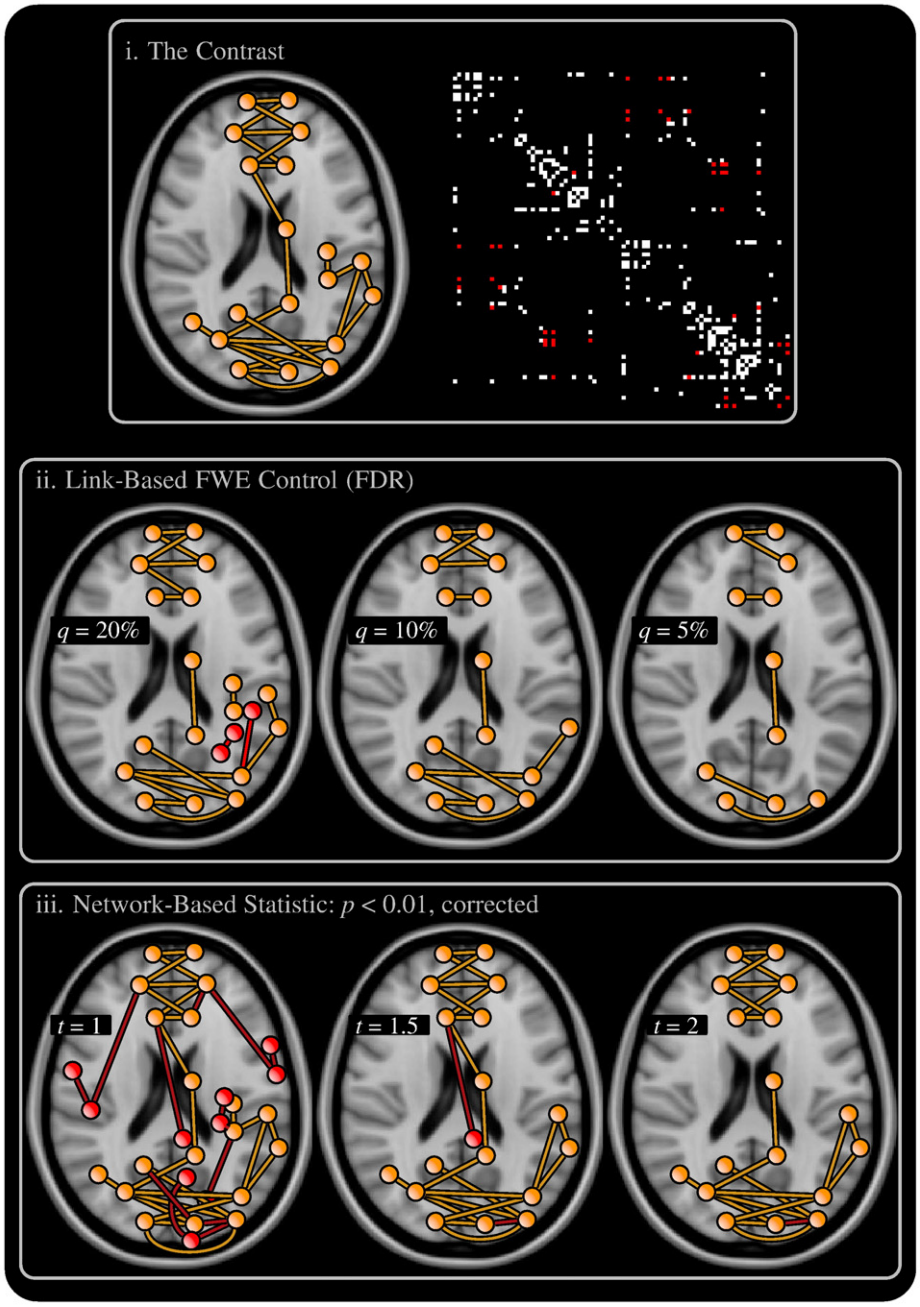

Fig. 2. The network-based statistic (NBS) as well as link-based FWE control provided by the false discovery rate (FDR) were used to detect a contrast that was simulated between two groups: (i) a connected component, referred to as the *contrast*, was disrupted in one of the groups to yield a contrast-to-noise ratio of unity between the two groups. The red blocks of the adjacency matrix indicate links comprising the contrast, while the white blocks indicate the other links that were tested but were not part of the contrast. (ii) The FDR was used to identify the component using false discovery rate thresholds of $q = 5$, 10 and 20%. (iii) The NBS was then used with primary (t-statistic) thresholds of $t = 1$, 1.5 and 2. True positives, colored orange, correspond to connections that were part of the contrast and correctly identified as such, while false positives, colored red, correspond to connections that were not part of the contrast but incorrectly identified as such. Each component identified by the NBS satisfied $p < 0.01$. With link-based FWE control, the full extent of the contrast only became evident for a liberal false discovery rate threshold. The true and [false] positive rates for each threshold were: FDR: $q = 5\%$: 0.3[0]; $q = 10\%$: 0.5[0]; $q = 20\%$: 0.7[0.006]; and NBS: $t = 1$: 1[0.08]; $t = 1.5$: 0.9[0.01]; $t = 2$: 0.9[0.006]. Nodes are depicted at their two-dimensional center of mass. The two components evident for $t = 2$ were each of sufficient size to be declared significant in their own right.

mean of zero. This yielded a contrast-to-noise ratio of unity. A t-statistic and corresponding p-value was then calculated for each link, after which the NBS and the FDR were used to identify the contrast (see caption of Fig. 2 for details). The graph model comprised a total of 82 nodes, each of which was extracted from the AAL atlas.

In Fig. 2, it can be seen that for even a very liberal FDR threshold of $q = 20\%$ (Genovese et al., 2002), link-based FWE control yielded a true positive rate of 0.7, with a false positive rate of 0.006. However, with the NBS, for $p = 0.01$ corrected, the true positive rate was 0.9, with a false positive rate of 0.006 ($t = 3$). It is crucial to remember though that this gain in power is at the cost of offering only weak control of the FWE.

Performance evaluation

Receiver operating characteristic (ROC) curves are presented in this section to evaluate the specificity and sensitivity of the NBS as well as link-based FWE control under a range of different network topologies, contrast extents and contrast-to-noise ratios. The FDR

served as the link-based controlling procedure, and thus any reference to FDR in this section is synonymous with link-based FWE control.

An ROC curve is a plot of the true positive rate (TPR) against the false positive rate (FPR), which is generated by varying the discrimination threshold over a continuous range. In the case of the NBS, the discrimination threshold is the minimum size of a component for it to be declared significant, while for the FDR, the q-value (Genovese et al., 2002) serves as the discrimination threshold. Ideal performance is indicated by a point in the upper left corner of the ROC curve, which represents 100% sensitivity (no false negatives) and 100% specificity (no false positives).

To construct an ROC curve, a contrast was simulated, corrupted with noise and then the NBS and the FDR were separately used to identify the contrast for a range of discrimination thresholds. The TPR was computed as $|\mathcal{P}\cap\hat{h}|/|\mathcal{P}|$ and the FPR was computed as $|\mathcal{N}\cap\hat{h}|/|\mathcal{N}|$, where $\mathcal{P}$ was the set of links comprising the contrast, $\mathcal{N}$ was the set of links comprising the rest of the network and $\hat{h}$ was the set of links declared significant. This was repeated independently for 10^3 trials and the average TPR and FPR was computed across the trials for each threshold. In this way, the TPR and FPR were parameterized in terms of the discrimination threshold. The TPR was then plotted as a function of the FPR in the range 0.001 to 0.05. An FPR exceeding 0.05 is most likely of no interest in a typical analysis and was therefore not considered, while an FPR below 0.001 was far too stringent to detect the contrast given the contrast-to-noise ratios evaluated.

The Barabási–Albert (BA) model (Albert & Barabási, 2002) was used to generate a random, scale-free network for each trial using a preferential attachment mechanism. A scale-free model was chosen because some studies have shown that brain networks are scale-free (Eguiluz et al., 2005; van den Heuvel et al., 2008), although it is important to remark that other studies have presented evidence for different degree distributions (Achard et al., 2006). The BA model is attractive because it is fully connected by construction, and it can be parameterized with only two variables, the number of nodes comprising the network, N, and a variable, m, which denotes the number of existing nodes to which a newly added node is attached to during each iteration of the preferential attachment mechanism. Hence, the number of links in the BA model is approximately Nm.

The next step was to create a contrast for each network. The contrast comprised a set of links that necessarily formed a connected component. The contrast was created by initiating a breadth first search (Ahuja et al., 1993) from a randomly chosen node in the network. Each link traversed during the search was included in the contrast and the search was terminated as soon as the contrast grew to reach its desired size.

Finally, a between group difference was created with respect to the contrast. In one group, the measure of association assigned to each link was sampled from a Gaussian distribution of zero mean and unity variance. In the other group, sampling was also from a Gaussian distribution of unity variance, but with a mean of μ if the link comprised the contrast, otherwise with a mean of zero. This yielded a contrast-to-noise ratio of μ.

The steps undertaken to construct an ROC curve can be summarized as follows:

(i) Generate a network with N nodes using the BA preferential attachment mechanism. Let $\mathcal{L}$ be the set of links comprising the network.
(ii) Initiate a breadth first search from a randomly chosen node to define a set of links, $\mathcal{P}\subset\mathcal{L}$, to serve as a contrast. Terminate the search as soon the contrast is of the desired size.
(iii) Let a_l be the measure of association at link $l\in\mathcal{L}$. In one group, sample such that $a_l\sim\mathbf{N}(0,1)$ for all $l\in\mathcal{L}$, which yields a noise-only network. In the other group, $a_l\sim\mathbf{N}(\mu,1)$ if $l\in\mathcal{P}$, otherwise $a_l\sim\mathbf{N}(0,1)$, which yields a noise + contrast network.
(iv) Perform mass-univariate testing for a between group difference; in particular, compute a t-statistic and corresponding p-value for each link.
(v) Use the NBS as well as link-based FWE control to yield an estimate, $\hat{h}$, of the set of links comprising the contrast for a range of discrimination thresholds.
(vi) For each discrimination threshold, compute $\text{TPR}=|\mathcal{P}\cap\hat{h}|/|\mathcal{P}|$ and $\text{FPR}=|\mathcal{N}\cap\hat{h}|/|\mathcal{N}|$.
(vii) Repeat the above for 10^3 trials to yield an average FPR and TPR.

Performance evaluation results

The ROC curves are presented in Figs. 3–5. Fig. 3 considers a contrast of 10 links embedded in a network comprising 100 nodes and 200 links ($m=2$) for contrast-to-noise ratios of: (i) 0.5, (ii) 1 and (iii) 1.5. A

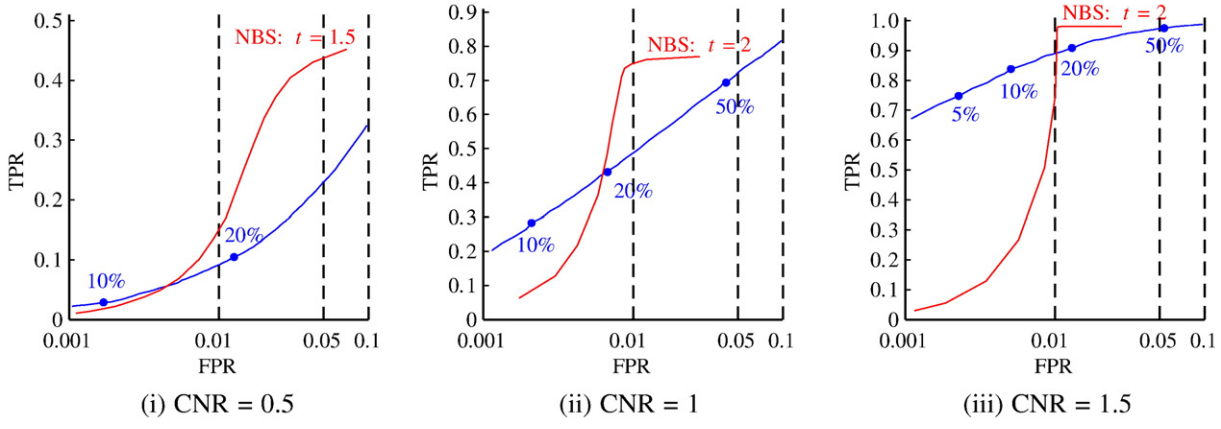

Fig. 3. Receiver–operator characteristic (ROC) curves were plotted to objectively compare the specificity and sensitivity of: the network-based statistic (NBS); and, link-based FWE control provided by the FDR. A separate ROC was plotted for three different contrast-to-noise ratios (CNR). To generate each ROC curve, the NBS and the FDR were used to detect a contrast that was simulated between two groups. In particular, a random, scale-free network of 100 nodes was generated and the connectivity in a component comprising 10 links was altered in one group to yield a CNR between the two groups of: (i) 0.5, (ii) 1 and (iii) 1.5. This was repeated 1000 times, each time generating a new random network and a new contrast. The average true positive rate (TPR) over the 1000 realizations was then plotted as function of the average false positive rate (FPR). Each point along the ROC curve for the FDR (colored blue) corresponds to a distinct q-value, some of which have been indicated as a percentage. For the NBS (colored red), each point represents a distinct component size threshold (i.e. components of size exceeding this threshold are declared significant). Observe that the NBS curve abruptly terminates and does not extend to an FPR of 0.1. This termination point represents the minimum possible component size threshold of unity.

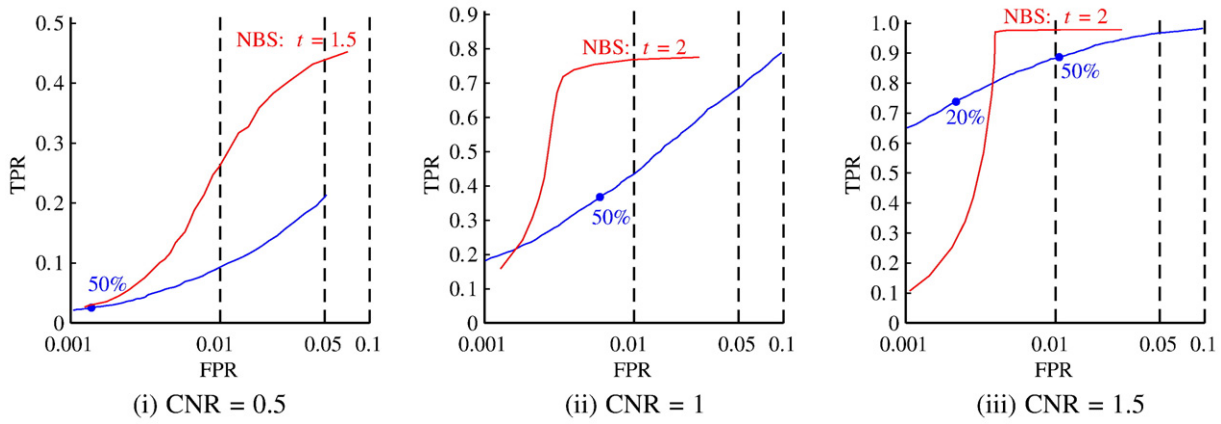

Fig. 4. The effect of a change in network size. In Fig. 3, the network comprised 100 nodes, 200 links and a contrast comprising 10 links. Here, the experiment was repeated for a larger network comprising 500 nodes and 1000 links, also with a contrast of 10 links. Therefore, the ratio of the total number of links to the number of links comprising the contrast was increased 5-fold from 200/10 = 20 to 1000/10 = 100. This figure demonstrates that the gain in power offered by the NBS increases with network size. See Fig. 3 caption for further details.

crossover point is evident for each ROC curve in Fig. 3. To the right of the crossover point, the NBS curve is higher than the FDR curve, signifying the NBS offers greater power over the range to the right of the crossover point. To the left of the crossover point, the opposite is true, and thus the FDR offers greater power over this range. The NBS clearly offers the greatest power over the TPR range probably of most interest, 0.5 to 1, although the advantage of the NBS declines as the contrast-to-noise ratio increases, until both approaches perform equally.

In Fig. 3, q-values have been indicated at strategic points along the FDR curve. The q-value is essentially the FDR analogue of the p-value, and is the minimum FDR at which significance is declared. The disadvantage of the FDR here is that a very high q-value ($q = 20$–50%) is required to achieve a reasonable FPR. For example, Fig. 3(ii) shows that a q-value threshold exceeding 20% is required to enforce a rather strict FPR of 0.01. This suggests that the FDR may be overly conservative in cases of low contrast-to-noise ratio.

Fig. 4 considers a substantially larger network than Fig. 3 to evaluate the effects of a change in network size. Specifically, Fig. 4 considers a contrast of 10 links embedded in a network comprising 500 nodes and 1000 links ($m = 2$) for the same set of contrast-to-noise ratios. Therefore, relative to Fig. 3, the ratio of the number of links comprising the contrast to the total number of links is reduced 100-fold from 10/100 to 10/1000. The same features are evident in Fig. 4; however, the crossover point is shifted further to the left and now occurs at an FPR well below 0.01. This indicates that the FPR range over which the NBS is favorable increases with network size.

Finally, Fig. 5 considers a change in network sparsity. In Fig. 3, the network sparsity was 4%. In Fig. 5, the sparsity is increased to (i) 2%, (ii) 8% and (iii) 16%. Sparsity was altered by including more links and maintaining the total number of nodes fixed at 100. In particular, the preferential attachment mechanism underlying the BA model was implemented with an increased value of m. Fig. 5 suggests that variations in sparsity impart a negligible effect.

The area under each ROC curve is shown in Supplementary Table S1.

While it is important to keep in mind that these conclusions do not necessarily generalize to problems of an arbitrary nature, it may be useful to summarize the key features evident in Figs. 3–5:

- The NBS is of no use if the contrast does not form a connected component. The following remarks pertain only to scenarios where the contrast *does* form a component.
- A single crossover point exists at which the NBS and the FDR offer equal power. The NBS offers greater power to the right of the crossover point. The right of the crossover point encompasses the TPR region of most interest, 0.5 to 1.
- As the contrast-to-noise ratio is increased, both the FDR and the NBS perform equally well.

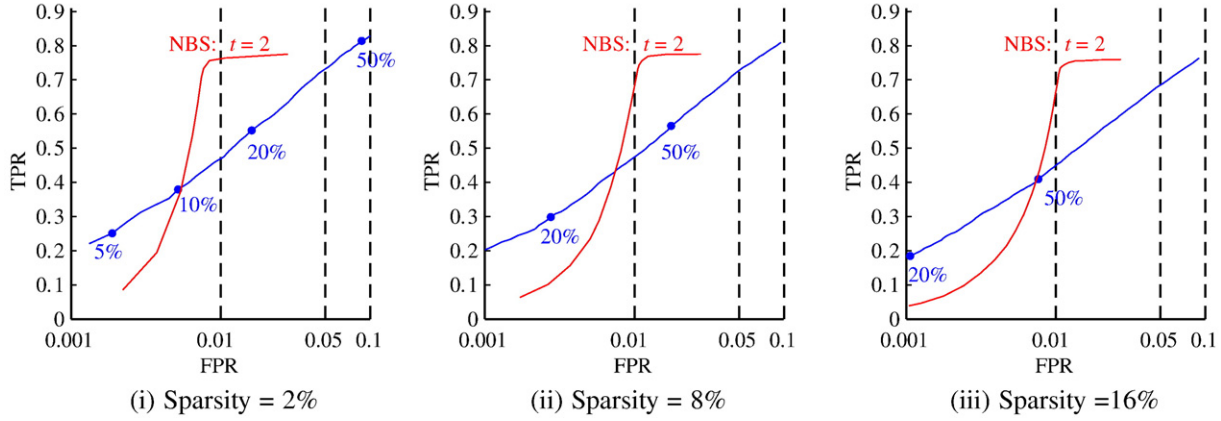

Fig. 5. The effect of a change in network sparsity. In Fig. 3, the network sparsity was 4% (100 nodes and 200 links). Here, the experiment was repeated for networks of sparsity: (i) 2%, (ii) 8% and (iii) 16%. Sparsity was altered by increasing the number of connections and maintaining the total number of nodes fixed at 100. A unity contrast-to-noise (CNR) ratio was used. This figure shows that the gain in power offered by the NBS is relatively unchanged to variations in sparsity. See Fig. 3 caption for further details.

- The gain in power offered by the NBS increases as the number of nodes and links is increased, with the contrast extent held constant, but is insensitive to variations in sparsity.
- A very high q-value ($q = 20$–50%) is required to operate over the range considered, indicating that the FDR may be overly conservative in cases of low contrast-to-noise ratio.

Finally, it is important to remark that the abscissa of each ROC curve is the expected proportion of false positives *per trial*. An alternative would have been to quantify the FPR as the proportion of trials for which there exists at least one false positive. Both definitions have distinct pros and cons. The former definition is the more conventional of the two and enables a better characterization of accuracy as well as requiring simulation of fewer trials. The main advantage of the latter definition is that it represents the strictest possible control of the FWE. The former definition may be considered more appropriate here given that the NBS is not intended to offer any control of the FWE at the level of individual links.

Application

The purpose of this section is to present new results derived from application of the NBS to a real case-control study involving a group of people with schizophrenia. In this section, a pair of nodes showing a weaker association in the group with schizophrenia is referred to as a *dysconnection* and the set of all such dysconnections is referred to as the *dysconnected subnetwork*.

Sample, data acquisition and processing

Sample characteristics

Fifteen healthy volunteers (mean age 33.3 years, $\sigma = 9.2$ years, 14 male) were recruited as well as 12 people with chronic schizophrenia (mean age 32.8 years, $\sigma = 9.2$ years, 10 male) diagnosed according to standard operational criteria in the Diagnostic and Statistical Manual of Mental Disorders IV (American Psychiatric Association, 2000). The two groups were matched for age, pre-onset IQ and years of education. All patients were receiving antipsychotic drugs. Four were receiving additional psychotropic medication. To reduce acute drug effects on the acquired data, patients did not receive their usual medication on the day of scanning. All subjects provided informed consent in writing and the protocol was approved by the Addenbrooke's NHS Trust Local Research Ethics Committee.

Acquisition

A 1.5 Tesla GE Signa scanner (General Electric, Milwaukee, WI) located at the BUPA Lea Hospital, Cambridge, UK, was used to acquire T_2^*-weighted echo-planar images depicting blood oxygenation level-dependent contrast as participants laid quietly in the scanner with eyes closed. Imaging parameters were as follow: repetition time: 2 s, echo time: 40 ms, flip angle: 70 degrees, voxel size: $3.05 \times 3.05 \times 7$ mm, slice gap: 0.7 mm, flip angle: 70 degrees, number of volumes: 512.

Processing and analysis

Each subject's functional volumes were realigned using a rigid-body transformation to correct for geometric displacements associated with head movements and rotations (Suckling et al., 2006). Temporal motion correction was then performed by regressing the current and lagged first and second order displacements against the time series of the realigned images. The residuals of this regression were then used for further analysis. These steps were implemented using freely available software (http://www-bmu.psychiatry.cam.ac.uk/software).

Nodes were delineated using a subset of the nodes comprising the AAL atlas. All nodes comprising the cerebellum were excluded as well as any nodes for which the node-averaged time series could not be accurately estimated, primarily due to poor coverage in one or more subjects. As such, a node-averaged time series was estimated in a total of 74 nodes spanning the cortex and subcortex.

The time series of each node was decomposed into four distinct frequency bands using the maximal overlap wavelet transform (Achard et al., 2006). For this paper, only scale 3 of the decomposition was considered, corresponding to the frequency range $0.03 < f < 0.06$ Hz, which is consistent with the range most commonly studied in resting-state functional MRI studies. These filtered time series were then corrected for fluctuations of nuisance signals of no interest via linear regression against reference time courses extracted from seed regions placed in the white matter and cerebrospinal fluid.

A 74×74 connectivity matrix was then populated for each subject, where the correlation in the preprocessed times series between the ith and the jth node was stored in element (i,j). A t-test contrasting the two groups was then computed for each pairwise association, based on the values stored in each subject's connectivity matrix. Any association with a t-statistic exceeding 3 was admitted to the set of suprathreshold links used by the NBS. The NBS was implemented as described in Section 2 and $M = 5000$ permutations were generated to estimate the null distribution of maximal component size.

To serve as a comparison, in a separate analysis, link-based FWE control was performed based on the p-values derived from the t-test. This corresponds to a conventional analysis that would be undertaken in the absence of the NBS. The FDR served as the link-based controlling procedure in this conventional analysis.

Dysconnected subnetwork

The NBS identified a single dysconnected subnetwork ($p = 0.037 \pm 0.005$, corrected) in the group with schizophrenia comprising 40 functional dysconnections. The confidence interval for the p-value was estimated parametrically as $2\sqrt{(p(1-p)/M)}$. Fig. 8 shows an axial schematic of the subnetwork, while Fig. 9 shows a three-dimensional visualization with both an oblique and axial perspective.

Table 1
Node abbreviations and degree.

Abbreviations	Node	Degree
PreC	Precentral L	2
	Precentral R	1
Rola	Rolandic Oper L	3
	Rolandic Oper R	4
SMA	Supp Motor Area L	7
	Supp Motor Area R	3
Cgl2	Cingulum Mid L	2
	Cingulum Mid R	1
Calc	Calcarine L	2
	Calcarine R	1
PstC	Postcentral L	6
	Postcentral R	2
Hesc	Heschl L	13
	Heschl R	1
Tem1	Temporal Sup L	1
	Temporal Sup R	1
Fro1	Frontal Sup L	1
Fro8	Frontal Inf Orb L	2
Fro9	Frontal Sup Medial L	1
Fro0	Frontal Med Orb L	6
Insu	Insula L	1
Cgl1	Cingulum Ant L	1
Hipp	Hippocampus L	3
Amy	Amygdala L	1
Cune	Cuneus L	3
Ling	Lingual R	3
Occ1	Occipital Sup L	5
Par1	Parietal Sup L	1
PCun	Precuneus L	2

Table 1 lists the nodes comprising the dysconnected subnetwork as well as their degree in this subnetwork, anatomical name and abbreviation.

When considering Figs. 8 and 9, it is important to remember that no individual dysconnection can be declared significant alone, only the dysconnected subnetwork as a whole can be declared significant. With respect to Fig. 8, it should additionally be noted that each node is positioned at its two-dimensional center of mass (left-right and anterior-posterior), resulting in no depth in the axial plane. This gives the illusion that the SMA nodes (supplementary motor area), for example, are located within the ventricles, which occurs simply because the axial slice chosen as the underlay is far more inferior than the SMA.

The dysconnected subnetwork identified with the NBS predominantly comprises fronto-temporal and occipito-temporal dysconnections, as well as SMA-temporal, SMA-occipital and the cingulum. While the dysconnected subnetwork is relatively bilateral, the left hemisphere is clearly affected to a greater extent. Indeed, the node from which the greatest number of dysconnections originate is the left Heschl's gyrus (Hesc), followed by the left post central gyrus (PstC) and the left SMA (see Table 1). Furthermore, the frontal regions implicated are exclusive to the left hemisphere, and thus the set of fronto-temporal dysconnections are asymmetric in the sense that the right temporal nodes show dysconnection with the left frontal nodes, but the converse is not evident.

The empirically computed null distribution of maximal component size is plotted in Fig. 6.

Comparison to link-based FWE control

For a rather liberal minimum FDR threshold of $q = 10\%$, link-based FWE control only identified a single dysconnection between the left post-central gyrus (PstC) and left rolandic operculum (Rola). This is in fact one of the dysconnections constituting the dysconnected subnetwork identified by the NBS. No significant findings were evident for the more commonly used threshold of $q = 5\%$. Fig. 7 depicts the dysconnections identified by the NBS and the FDR in the form of separate adjacency matrices. A dysconnection is shown as a white block, while all other connections are colored black.

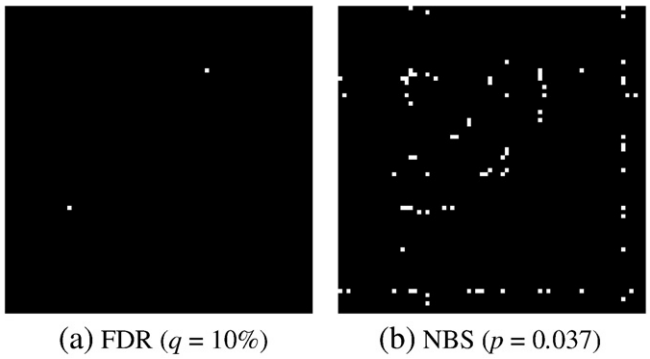

Fig. 7. Adjacency matrices showing dysconnections (white blocks) in the group with schizophrenia identified with: (a) link-based FWE control provided by the FDR; and, (b) the NBS. The FDR identified a single dysconnection between the left post-central gyrus (PstC) and left rolandic operculum (Rola), while the NBS identified a single dysconnected subnetwork primarily comprising fronto-temporal and occipito-temporal dysconnections (see Fig. 8).

Discussion

With continuing popularization of the graph model in all kinds of neuroimaging research, we believe there is a need for statistical approaches to identify connections in this model that may be associated with an effect or contrast of interest; for example, diagnostic status in a case-control comparison, a difference due to changing task conditions in a functional paradigm, pharmacological modulation, or correlation with some external behavioral measure. While mass-univariate testing is an option, the enormous number of multiple comparisons involved, together with a potentially low contrast-to-noise ratio, means that this approach may be underpowered. The NBS is a new option that can offer substantially greater power if the connections associated with the contrast or effect of interest are interconnected to form a structure; or more precisely, a connected component. The underlying principle behind the NBS is to utilize the presence of any such components to potentially yield greater power than what is possible by independently correcting the p-values computed for each connection comprising the graph with a generic procedure such as the FDR (Figs. 8 and 9).

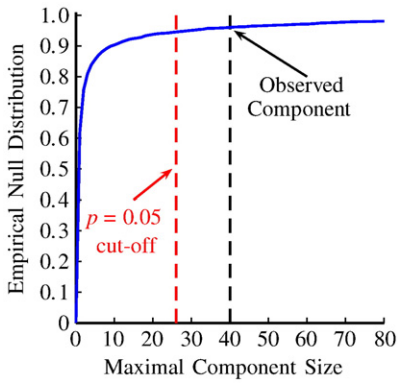

Fig. 6. Empirically computed null distribution of maximal component size. The component identified in the real data comprised 40 connections.

But is the NBS really necessary? Indeed, if the contrast-to-noise ratio is sufficiently high, generic procedures that operate on the link-based p-values alone can presumably provide enough power to declare the effect of interest significant. Moreover, generic procedures such as the FDR offer three distinct advantages over the NBS. Foremost, the NBS must be used under the assumption that the connections comprising the contrast of interest form components. If they do not form components, or if the extent of the components formed are too small, the NBS is ineffective, whereas generic procedures providing link-based FWE control do not require any such assumption. Secondly, the NBS only offers weak control of the FWE; that is, with the NBS, only the omnibus null hypothesis for a component can be rejected, but the individual connections comprising a component can never be declared significant. In this way, the NBS provides coarser localizing power. And thirdly, when using the NBS, a rather arbitrary choice must be made to select the value of the threshold used to define the set of suprathreshold links.

So why use the NBS, given that its localizing power is coarser and it necessitates an assumption on the interconnectedness of the contrast? Firstly, we believe that the assumptions on which the NBS is based are implicit in a typical network analysis of neuroimaging data. In particular, the hypothesis tested usually involves examination of effects distributed across various components of information-processing pathways. While it is possible for highly focal effects to exist in a given network, most networks, being interconnected by definition, are likely to show secondary consequences of any focal effects that can propagate along interconnected pathways. Thus, most effects are likely to influence interconnected subnetworks that the NBS is well suited to detecting.

The second reason is simply a matter of power—the NBS can offer substantially greater power in the right circumstances, which is

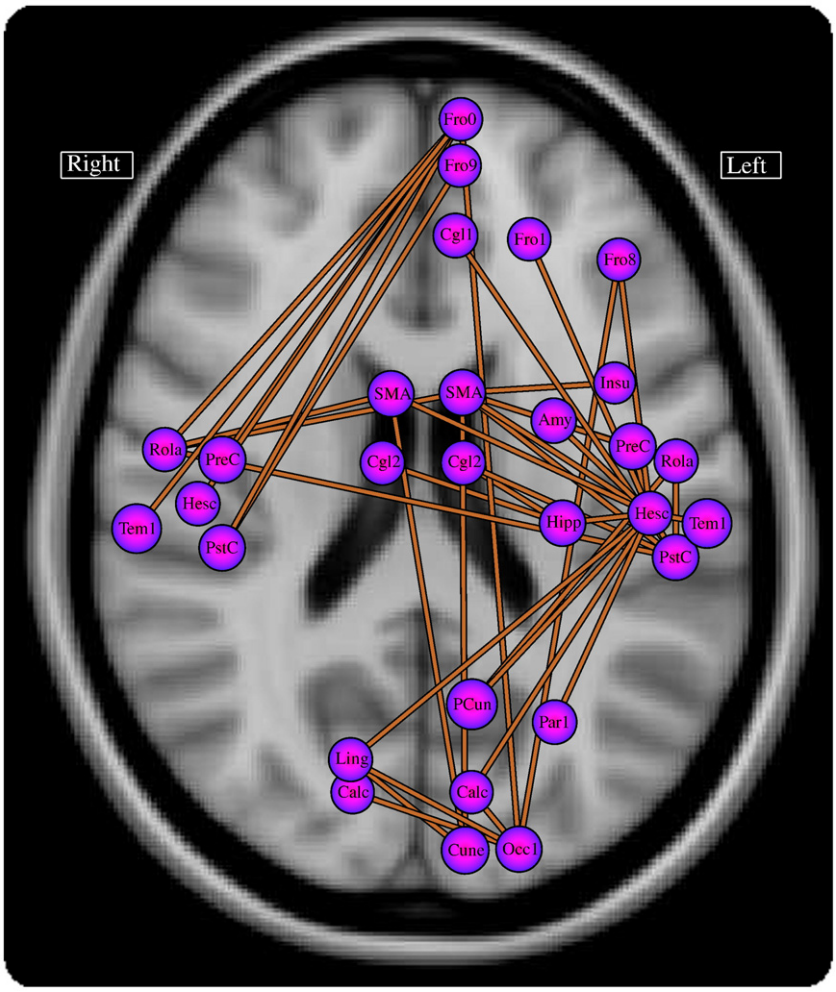

Fig. 8. The NBS identified a dysconnected functional subnetwork ($p = 0.037 \pm 0.005$, corrected) in a group of 12 people with schizophrenia. The dysconnections comprising this subnetwork correspond to pairs of nodes between which the resting-state times series (wavelet decomposed) was more weakly correlated in the group with schizophrenia than in the control group. It is important to emphasize that no individual dysconnection can be declared significant alone, only the dysconnected subnetwork as a whole can be declared significant. Each node is depicted as a circle positioned at its center of mass. See Table 1 for node abbreviations.

advantageous in the context of the graph model due to the massive number of multiple comparisons that arise when the hypothesis of interest is tested at every connection. To appreciate the massiveness of the multiple comparisons problem, an example was given where it was shown that the number of multiple comparisons scaled polynomially with the number of voxels of interest, namely $\mathcal{O}(N^2)$, whereas the number of multiple comparisons performed in a statistical parametric map is linear in the number of voxels of interest. Therefore, due to this massive increase, the contrast-to-noise ratio ought to be very high if a generic procedure is to have any chance of declaring the contrast significant. Unfortunately, the range of measures available to quantify pairwise associations between nodes is derived from MRI data or other experimental imaging modalities, which are invariably noisy. It is thus inevitable for this noise to propagate to the measure of association, potentially resulting in a low contrast-to-noise ratio. For example, the number of interconnecting streamlines, a measure of anatomical connectivity derived from diffusion MRI, is notoriously noisy due to artifacts stemming from tractography (Zalesky & Fornito, 2009).

As such, a conventional mass-univariate analysis within the framework of the graph model may not be able to provide sufficient power. This lack of power motivated the development of the NBS. The NBS is founded on the same principle underlying traditional cluster-based thresholding of statistical parametric maps. The main difference is that graph components play the role of voxel clusters.

With the NBS, the link-based *p*-values corresponding to the contrast or effect of interest need not be so significant as to survive in a sea of potentially hundreds of thousands of multiple comparisons (as would be required by the FDR). Instead, they only need to be significant enough to be admitted into the set of suprathreshold links, and assuming they are interconnected to form a sufficiently large component (or components), they can be declared significant. In a mass-univariate analysis controlled with the FDR though, to survive in a sea of hundreds of thousands of multiple comparisons, the contrast-to-noise ratio would need to be high in order to yield very significant link-based *p*-values.

An advantage of the NBS is that its power may scale with the size of the network. Suppose the cortex is coarsely subdivided into a total of 10 nodes, and the NBS as well as conventional mass-univariate testing identify a significant effect involving say three connections giving rise to a component of extent three. For a coarse subdivision such as this, a node is likely to encompass several functionally distinct regions, and thus any dysconnections between regions that are lumped together within a common node cannot be identified because they are simply not modeled. Now suppose the cortex is subdivided more finely into a total of 1000 nodes. The number of multiple comparisons increases from 45 to 499,500, and thus a mass-univariate analysis may not have sufficient power to detect the effect unless the contrast-to-noise ratio is high. The NBS is also likely to have difficulty in identifying

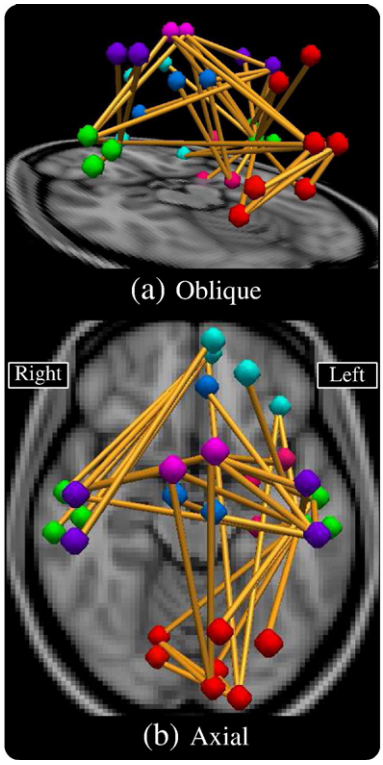

Fig. 9. Three-dimensional visualization of the dysconnected functional subnetwork identified with the NBS in a group of 12 people with schizophrenia. See caption of Fig. 8 for details. Red: occipital/parietal nodes. Green: temporal nodes. Purple: pre and post central gyrus. Light blue: frontal nodes. Blue: cingulum. Magenta: Supp. Motor Area.

a component of extent three in a network comprising 499,500 connections, for the possibility of a component of larger or equal extent arising as a matter of chance increases dramatically relative to the 10 node case. However, the effect is likely to be more extensive now and therefore easier to detect because dysconnections between nodes that were previously lumped together within a common node now arise. In other words, although the multiple comparisons problem is exacerbated as the size of the network is increased, the extent of the contrast or effect of interest is also likely to scale up with network size.

The NBS attempts to exploit the interconnected nature of link-based effects, as revealed through mass univariate testing. This makes the approach relatively simple to implement and interpret. However, brain connectivity data are inherently multivariate in nature. As such, multivariate methods may provide added sensitivity for detecting alterations of connectivity under various conditions. In a multivariate version of the NBS, functional as well as anatomical measures of connectivity can be combined, for example, by computing Hotelling's T^2 statistic at each link.

Finally, it is important to make clear that it is difficult to provide definitive rules guiding how to choose the set of suprathreshold links. If the threshold is chosen too low, large components can arise in the permuted data as a matter of chance and thereby reduce power. In contrast, if the threshold is set too high, connections comprising the effect of interest may not be admitted to the set of suprathreshold links. In Section 3, the thresholds used for the NBS were chosen rather arbitrarily; namely, $t=1.5$ if the contrast-to-noise ratio was below unity and $t=2$ otherwise. It is possible that the performance of the NBS could have been improved in this study by 'optimizing' the threshold selection with trial and error. An approach to avoid the problem of threshold selection was recently proposed by Smith & Nichols (2009) in the context of cluster-based statistics.

Schizophrenia findings

The dysconnected functional subnetwork identified in the group of people with schizophrenia involved fronto-temporal dysconnectivity of the left hemisphere, but also extended to incorporate, parietal and occipital regions, in which the group with schizophrenia showed reduced connectivity relative to controls. This finding is in line with recent meta-analyses of structural imaging studies in schizophrenia, suggesting that the most robust grey-matter changes occur in frontal, temporal, subcortical and parietal regions, most prominently in the left hemisphere (Ellison-Wright et al., 2008; Fornito et al., 2009). They are also consistent with functional MRI evidence of disturbed fronto-temporal connectivity in patients (Fletcher et al., 1999), which may result from genetic risk for the disorder (Esslinger et al., 2009), and diffusion MRI studies suggesting a disruption of tracts connecting frontal, temporal and occipital regions (Ellison-Wright & Bullmore, 2009). Thus, while the interpretation of case-control differences in resting-state functional MRI data may not always be straightforward (Fornito & Bullmore, 2010), the NBS identified a core network of reduced functional connectivity that is consistent with pathological alterations reported in the literature, as identified using a variety of imaging modalities.

Conclusion

This paper presented a new approach, called the network-based statistic (NBS), to identify functional or structural connectivity differences in neuroimaging data that is modeled as a network. With the use of receiver operating characteristic (ROC) curves, the NBS was shown to yield substantially greater statistical power than generic procedures for controlling the FWE, as long as any connectivity differences were structured in such a way that they formed connected components. The fact that the NBS can only provide weak control of the family-wise error rate was recognized as its main disadvantage. The utility of the NBS was then demonstrated in the context of a real case-control study involving 12 people with chronic schizophrenia and 15 controls for which resting-state functional MRI data was acquired. The NBS identified a single dysconnected subnetwork in the group with schizophrenia that predominantly comprised fronto-temporal and occipito-temporal dysconnections. We believe the NBS will play an important role in the network analysis of neuroimaging data.

Acknowledgments

We are grateful for the assistance provided by Dr Manfred Kitzbichler and Dr Ulrich Müller in acquiring and preprocessing the MRI data used to validate our algorithm in Section 4. AZ is supported by the Australian Research Council (DP0986320). AF is supported by a National Health and Medical Research Council CJ Martin Fellowship (ID: 454797).

Appendix A. Supplementary data

Supplementary data associated with this article can be found, in the online version, at 10.1016/j.neuroimage.2010.06.041.

References

Achard, S., Salvador, R., Whitcher, B., Suckling, J., Bullmore, E., 2006. A resilient, low-frequency, small-world human brain functional network with highly connected association cortical hubs. J. Neurosci. 26 (1), 63–72.
Ahuja, R.K., Magnanti, T.L., Orlin, J.B., 1993. Network flows: theory algorithms and applications. Prentice Hall.
Albert, R., Barabási, A.-L., 2002. Statistical mechanics of complex networks. Rev. Mod. Phys. 74, 47–97.
Basser, P.J., Pajevic, S., Pierpaoli, C., Duda, J., Aldroubi, A., 2000. In vivo fiber tractography using DT-MRI data. Magn. Reson. Med. 44, 625–632.

Bassett, D.S., Bullmore, E., Verchinski, B.A., Mattay, V.S., Weinberger, D.R., Meyer-Lindenberg, A., 2008. Hierarchical organization of human cortical networks in health and schizophrenia. J. Neurosci. 28 (37), 9239–9248.
Bassett, D.S., Bullmore, E.T., Meyer-Lindenberg, A., Apud, J.A., Weinberger, D.R., Coppola, R., 2009. Cognitive fitness of cost-efficient brain functional networks. PNAS 106 (28), 11747–11752.
Bullmore, E., Barnes, A., Bassett, D.S., Fornito, A., Kitzbichler, M., Meunier, D., Suckling, J., 2009. Generic aspects of complexity in brain imaging data and other biological systems. Neuroimage 47 (3), 1125–1134.
Bullmore, E., Sporns, O., 2009. Complex brain networks: graph theoretical analysis of structural and functional systems. Nat. Rev. Neurosci. 10, 186–198.
Bullmore, E.T., Suckling, J., Overmeyer, J., Rabe-Hesketh, S., Taylor, E., Brammer, M.J., 1999. Global, voxel and cluster tests, by theory and permutation, for differences between two groups of structural MR images of the brain. IEEE Trans. Med. Imaging 18, 32–44.
Conturo, T.E., Lori, N.F., Cull, T.S., Akbudak, E., Snyder, A.Z., Shimony, J.S., McKinstry, R.C., Burton, H., Raichle, M.E., 1999. Tracking neuronal fiber pathways in the living human brain. Proc. Natl Acad. Sci. USA 96 (18), 10422–10427.
Deuker, L., Bullmore, E., Smith, M., Christensen, S., Nathan, P.J., Rockstroh, B., Basset, D.S., 2009. Reproducibility of graph metrics of human brain functional networks. Neuroimage 47 (4), 1460–1468.
Eguiluz, V.M., Chialvo, D.R., Cecchi, G.A., Baliki, M., Apkarian, A.V., 2005. Scale-free brain functional networks. Phys. Rev. Lett. 94 (1), 018102.
Ellison-Wright, I., Glahn, D.C., Laird, A.R., Thelen, S.M., Bullmore, E., 2008. The anatomy of first-episode and chronic schizophrenia: an anatomical likelihood estimation meta-analysis. Am. J. Psychiatry 165, 1015–1023.
Ellison-Wright, I., Bullmore, E., 2009. Meta-analysis of diffusion tensor imaging studies in schizophrenia. Schizophr. Res. 108, 3–10.
Esslinger, C., Walter, H., Kirsch, P., Erk, S., Schnell, K., Arnold, C., Haddad, L., Mier, D., Opitz von Boberfeld, C., Raab, K., Witt, S.H., Rietschel, M., Cichon, S., Meyer-Lindenberg, A., 2009. Neural mechanisms of a genome-wide supported psychosis variant. Science 324 (5927), 605.
Fair, D.A., Cohen, A.L., Power, J.D., Dosenbach, N.U.F., Church, J.A., Miezin, F.M., Schlaggar, B.L., Petersen, S.E., 2009. Functional brain networks develop from a "local to distributed" organization. PLoS Comput. Biol. 5, e1000381.
Fletcher, P., McKenna, P.J., Friston, K.J., Frith, C.D., Dolan, R.J., 1999. Abnormal cingulate modulation of fronto-temporal connectivity in schizophrenia. Neuroimage 9, 337–342.
Fornito, A., Bullmore, E.T., 2010. What can spontaneous fluctuations of the blood oxygenation-level-dependent signal tell us about psychiatric disorders? Curr. Opin. Psychiatry 23, 239–249.
Fornito, A., Yucel, M., Patti, J., Wood, S.J., Pantelis, C., 2009. Mapping grey matter reductions in schizophrenia: an anatomical likelihood estimation analysis of voxel-based morphometry studies. Schizophr. Res. 108, 104–113.
Fornito, A., Yoon, J., Zalesky, A., Firl, A., Ooms, R., Bullmore ET, Carter C., 2010. Disrupted fronto-posterior connectivity during cognitive control in first episode schizophrenia revealed by event-related graph analysis. Poster Presentation. Schizophrenia International Research Society (SIRS) Congress, Florence, Italy. April 10-14.
Genovese, C.R., Lazar, N.A., Nichols, T., 2002. Thresholding of statistical maps in functional neuroimaging using the false discovery rate. Neuroimage 15, 870–878.
Gong, G., Rosa-Neto, P., Carbonell, F., Chen, Z.J., He, Y., Evans, A.C., 2009. Age- and gender-related differences in the cortical anatomical network. J. Neurosci. 29 (50), 15684–15693.
Hagmann, P., Kurant, M., Gigandet, X., Thiran, P., Wedeen, V.J., Meuli, R., Thiran, J.-P., 2007. Mapping human whole-brain structural networks with diffusion MRI. PLoS ONE 2 (7), e597.
Hagmann, P., Cammoun, L., Gigandent, X., Meuli, R., Honey, C.J., Wedeen, V.J., Sporns, O., 2008. Mapping the structural core of the human cerebral cortex. PLoS Biol. 6 (7), e159.
Hayasaka, S., Nichols, T.E., 2004. Combining voxel intensity and cluster extent with permutation test framework. Neuroimage 23, 54–63.
Hayasaka, S., Laurienti, P.J., 2010. Comparison of characteristics between region- and voxel-based network analyses in resting-state fMRI data. Neuroimage 50, 499–508.
He, Y., Chen, Z., Evans, A., 2007. Small-world anatomical networks in the human brain revealed by cortical thickness from MRI. Cereb. Cortex 17, 2407–2419.
He, Y., Chen, Z.J., Evans, A.C., 2008. Structural insights into aberrant topological patterns of large-scale cortical networks in Alzheimer's disease. J. Neurosci. 28 (18) 4756-4766.
He, Y., Dagher, A., Chen, Z., Charil, A., Zijdenbos, A., Worsley, K., Evans, A., 2009. Impaired small-world efficiency in structural cortical networks in multiple sclerosis associated with white matter lesion load. Brain 132 (12), 3366–3379.
Honey, C.J., Sporns, O., Cammoun, L., Gigandet, X., Thiran, J.-P., Meuli, R., Hagmann, P., 2009. Predicting human resting-state functional connectivity from structural connectivity. PNAS 106 (6), 2035–2040.
Honey, C.J., Thivierge, J.-P., Sprons, O., 2010. Can structure predict function in the human brain? Neuroimage. doi:10.1016/j.neuroimage.2010.01.071.
Hopcroft, J., Tarjan, R., 1973. Efficient algorithms for graph manipulation. Commun. ACM 16, 372–378.
Itturia-Medina, Y., Sotero, R.C., Canales-Rodríguez, E.J., Alemán-Gómez, Y., Melie-García, L., 2008. Studying the human brain anatomical network via diffusion-weighted MRI and graph theory. Neuroimage 40 (3), 1064–1076.
Li, Y., Liu, Y., Li, J., Qin, W., Kuncheng, L., Yu, C., Jiang, T., 2009. Brain anatomical network and intelligence. PLoS Comput. Biol. 5 (1), e1000395.
Liu, Y., Liang, M., Zhou, Y., He, Y., Hao, Y., Song, M., Yu, C., Liu, H., Liu, Z., Jiang, T., 2008. Disrupted small-world networks in schizophrenia. Brain 131, 945–961.
Nichols, T.E., Holmes, A.P., 2001. Nonparametric permutation tests for functional neuroimaging: a primer with examples. Hum. Brain Mapp. 15, 1–25.
Nichols, T., Hayasaka, S., 2003. Controlling the familywise error rate in functional neuroimaging: a comparative review. Stat. Meth. Med. Res. 12 (5), 419–446.
Ramani, N., Behrens, T.E.J., Penny, W., Matthews, P.M., 2004. New approaches for exploring anatomical and functional connectivity in the human brain. Biol. Psychiatry 56 (9), 613–619.
Robinson, E.C., Hammers, A., Ericsson, A., Edwards, A.D., Rueckert, D., 2010. Identifying population differences in whole-brain structural networks: a machine learning approach. Neuroimage 50, 910–919.
Rubinov, M., Knock, S.A., Stam, C.J., Micheloyannis, S., Harris, A.W.F., Williams, L.M., Breakspear, M., 2009. Small-world properties of nonlinear brain activity in schizophrenia. Hum. Brain Mapp. 30, 403–416.
Skudlarski, P., Jagnnathan, K., Calhoun, V.D., Hampson, M., Skudlarska, B.A., Pearlson, G., 2008. Measuring brain connectivity: diffusion tensor imaging validates resting state temporal correlations. Neuroimage 43, 554–561.
Smith, S.M., Nichols, T.E., 2009. Threshold-free cluster enhancement: addressing problems of smoothing, threshold dependence and localisation in cluster inference. Neuroimage 44, 83–98.
Sporns, O., Tononi, G., Edelman, G.M., 2000. Theoretical neuroanatomy: relating anatomical and functional connectivity in graphs and cortical connection matrices. Cereb. Cortex 10, 127–141.
Sporns, O., Chialvo, D.R., Kaiser, M., Hilgetag, C.C., 2004. Organization, development and function of complex brain networks. Trends Cogn. Sci. 8 (9), 418–425.
Stam, C.J., Jones, B.F., Nolte, G., Breakspear, M., Scheltens, P., 2007. Small-world networks and functional connectivity in Alzheimer's disease. Cereb. Cortex 17, 92–99.
Suckling, J., Bullmore, E., 2004. Permutation tests for factorially designed neuroimaging experiments. Hum. Brain Mapp. 22, 193–205.
Suckling, J., Long, C., Triantafyllou, C., Brammer, M., Bullmore, E., 2006. Variable precision registration via wavelets: optimal spatial scales for inter-subject registration of functional MRI. Neuroimage 31 (1), 197–208.
Tzourio-Mazoyer, N., Landeau, B., Papathanassiou, D., Crivello, F., Etard, O., Delcroix, N., Mazoyer, B., Joliot, M., 2002. Automated anatomical labeling of activations in SPM using a macroscopic anatomical parcellation of the MNI MRI single-subject brain. Neuroimage 15 (1), 273–289.
van den Heuvel, M.P., Stam, C.J., Boersma, M., Hulshoff Pol, H.E., 2008. Small-world and scale-free organization of voxel-based resting-state functional connectivity in the human brain. Neuroimage 43, 528–539.
van den Heuvel, M.P., Stam, C.J., Kahn, R.S., Hulshoff Pol, H.E., 2009. Efficiency of functional brain networks and intellectual performance. J. Neurosci. 29 (23), 7619–7624.
Wang, L., Li, Y., Metzak, P., He, Y., Woodward, T.S., 2010. Age-related changes in topological patterns of large-scale brain functional networks during memory encoding and recognition. Neuroimage 50, 862–872.
Wang, L., Zhu, C., He, Y., Zang, Y., Cao, Q., Zhang, H., Zhong, Q., Wang, Y., 2009. Altered small-world brain functional networks in children with attention-deficit/hyperactivity disorder. Hum. Brain Mapp. 30 (2), 638–649.
Zalesky, A., Fornito, A., 2009. A DTI-derived measure of cortico-cortical connectivity. IEEE Trans. Med. Imaging 28 (7), 1023–1036.
Zalesky, A., Fornito, A., Harding, I.H., Cocchi, L., Yucel, M., Pantelis, C., Bullmore, E.T., 2010. Whole-brain anatomical networks: does the choice of nodes matter? Neuroimage 50 (3), 970–983.